Chapter 2

2. Instrumentation, Materials and Methodology

2.1 Instrumentation

In the field of experimental research, the role of the instruments is paramount. The instruments facilitate the conversion of theoretical hypotheses into quantifiable and verifiable data. Instruments enable researchers to observe, measure, and analyze phenomena on scales that are otherwise beyond the reach of unaided senses. The precise selection, calibration, and application of these tools are essential to ensure the accuracy and reliability of experimental results. In this section, I discuss the key instruments employed in this study, briefly explaining their working principle, key components, and significance in achieving rigorous research outcomes.

2.1.1 UV-Vis Spectroscopy

UV-Vis spectroscopy is an analytical technique employed to examine the absorbance of ultraviolet and visible light by a sample. This technique is grounded in the principle that molecules absorb light at specific wavelengths, corresponding to electronic transitions between molecular orbitals. When a sample is exposed to UV or visible light, certain wavelengths are absorbed, and the resulting spectrum provides valuable insights into the sample's properties. The working principle of UV-Vis spectroscopy involves the interaction of light with the sample. As light passes through the sample, photons with energy matching the energy gap between electronic states are absorbed. This absorption leads to electronic excitations, and the intensity of absorbed light is measured as a function of wavelength.

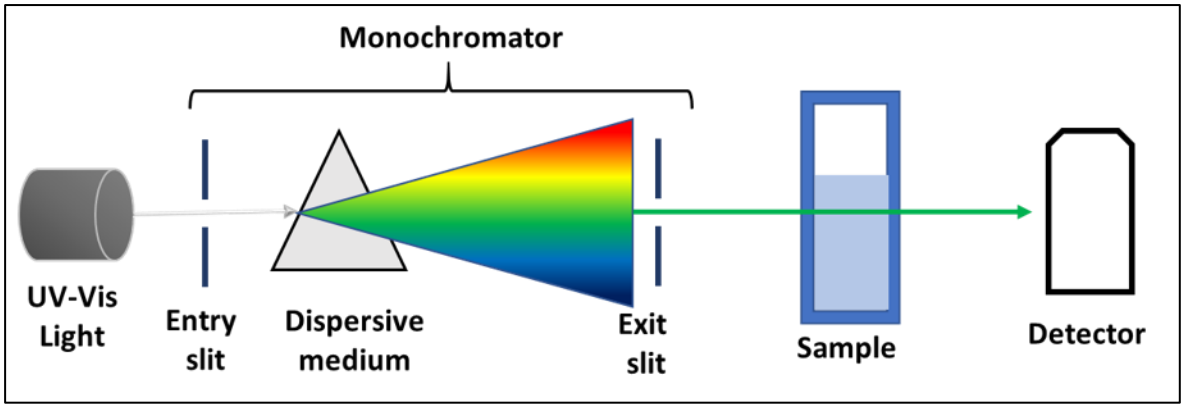

Figure 2.1 Schematic for UV Vis single beam spectrometer.

The absorbance (A) is calculated using Beer-Lambert's law, which relates absorbance to I_0 and I, the intensity of the incident and transmitted light, the concentration (c) of the absorbing species, the path length (l), and the molar absorptivity (ε):

$$A = \log_{10} \frac{I_0}{I} = \varepsilon c l$$

A UV-Vis spectrometer is composed of three components: a light source that produces light in the range of UV and visible spectra, a monochromator that disperses the light into its constituent wavelengths and sends a specific wavelength through the sample, and a detector that measures the intensity of light before and after it passes through the sample (**Figure 2.1**). The detector then converts the light into an electrical signal, which is then analyzed. This instrument's versatility, precision and non-destructive nature makes it vital for application in several scientific fields. It is widely used to determine the concentration of analytes in a solution, study reaction kinetics, and analyze the purity of compounds.

2.1.2 Fourier Transform Infrared Spectroscopy

Fourier Transform Infrared (FTIR) spectroscopy is a powerful analytical technique used to obtain the infrared spectrum of absorption or emission of a solid, liquid, or gas. This method provides detailed information about molecular vibrations and the chemical

composition of a sample, making it indispensable in both qualitative and quantitative analysis. FTIR spectroscopy is based on the principle that molecules absorb specific frequencies of infrared light that correspond to the vibrational modes of the molecular bonds. When infrared radiation passes through a sample, specific wavelengths are absorbed, resulting in a spectrum representing the sample's molecular fingerprint. An FTIR spectrometer uses an interferometer, which generates a signal produced by constructive and destructive interference of the two beams of light. This signal is subjected to Fourier transform, which converts the time-domain data into a frequency-domain spectrum, revealing the absorption peaks corresponding to different vibrational modes. FTIR spectrometer comprises the following components; an interferometer, a sample compartment, a detector, and a computer with a Fourier transform processor for data analysis (**Figure 2.2a**).

FTIR spectroscopy is significant in a wide range of applications due to its ability to provide detailed molecular information rapidly and non-destructively. It is helpful in identifying the functional groups and chemical structures of organic and inorganic materials.

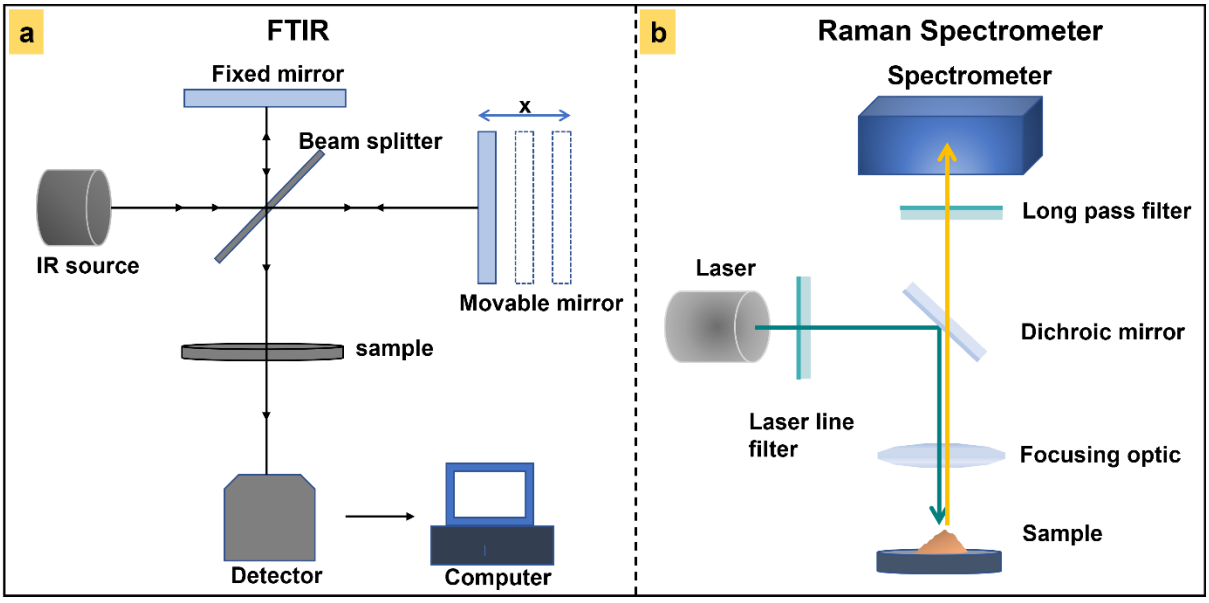

Figure 2.2 Schematic diagram of **(a)** Fourier transform infrared spectrometer and **(b)** Raman spectrometer**.**

2.1.3 Raman Spectroscopy

Raman spectroscopy is another powerful technique that relies on studying vibrational, rotational, and other low-frequency modes in a molecular system to gain knowledge regarding chemical bonding, molecular structure, and crystallinity of materials. It relies on the inelastic scattering of monochromatic light by molecules. When photons from a light source interact with a sample, most scatter elastically (known as Rayleigh scattering), while a small fraction undergoes inelastic scattering. This results in a shift in the energy of the scattered photons, which corresponds to the vibrational energy levels of the molecules. The resulting Raman spectrum represents the molecular fingerprint of the sample, showing peaks corresponding to different vibrational modes. The key components of a Raman spectrometer include a laser source for exciting the molecules, a sample holder, a monochromator or grating for wavelength selection, a detector (such as charged coupled device (CCD) or photomultiplier tube (PMT)), and a computer with spectral analysis for data processing and analysis (**Figure 2.2b**). This technique is exclusively used in various

scientific fields for its ability to provide detailed information non-destructively and rapidly. In chemistry, it is used to identify and characterize unknown substances, study molecular conformations, and monitor chemical reactions in real time. It is also heavily used in material science for analyzing polymers, nanomaterials, semiconductors, and biomaterials. This technique is specifically advantageous owing to its high sensitivity, rapid analysis, and requirement of minimal sample preparation.

2.1.4 X-Ray Diffraction

X-ray Diffraction (XRD) is a widely used analytical technique for characterizing materials' crystallographic structure, composition, and physical properties. XRD relies on the principle of constructive interference of monochromatic X-rays and a crystalline sample. Many materials are made up of small crystallites, and depending on their chemical composition and structural type, these materials can coexist in multiple crystallite phases simultaneously. When X-ray light is incident on the material, different crystallites diffract it in various directions as per Bragg's law:

$$n\lambda = 2dSin(\theta)$$

Where n is an integer, λ is the wavelength of the incident X-rays, d is the interplanar distance, and θ is the angle of incidence at which diffraction occurs. By measuring the angles and their corresponding intensities of the diffracted beams, the interplanar distance between lattice planes of the material can be determined, which is key information for knowing the crystal structure. In a typical XRD instrument, X-rays are produced by a rotating or sealed tube X-ray generator. A sample holder positions the sample in the X-ray beam path. The goniometer controls the angle of incidence and diffraction, which rotates

the sample and detector around a common axis. Finally, the sensor captures the diffracted X-rays and measures their intensity, which is further processed with the help of a computer to interpret the crystal structure (**Figure 2.3a**).

XRD is a crucial technique for the analysis of material structure both in scientific and industrial applications. It helps identify phase compositions, detect crystallographic defects, and determine crystallite size. It is also utilized in pharmaceuticals to assess the purity and consistency of drugs.

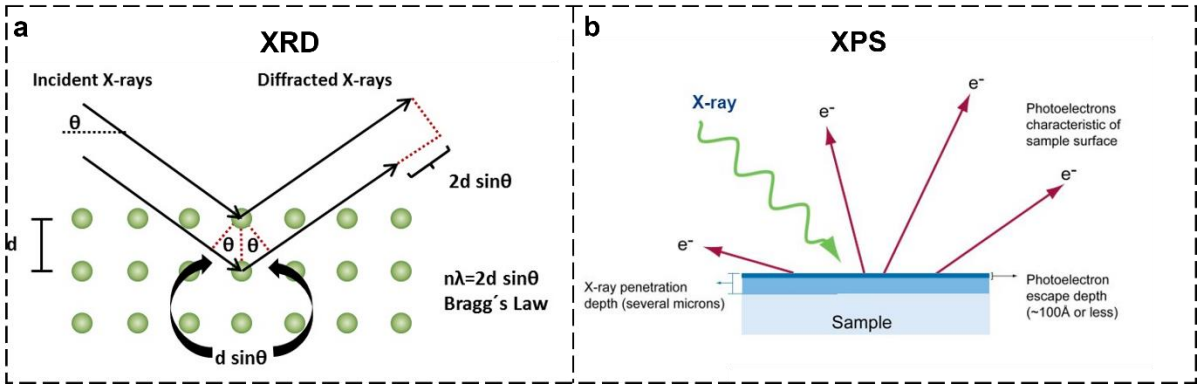

Figure 2.3 Schematic diagram showcasing working principle for **(a)** X-ray diffraction technique and **(b)** X-ray photoelectron spectroscope. (Credit: *https://wiki.anton-paar.com/se-en/x-ray-diffraction-xrd/*)

2.1.5 X-ray Photoelectron Spectroscopy

X-ray Photoelectron Spectroscopy (XPS) is a highly sensitive surface analysis technique used to investigate the elemental composition, chemical state, and electronic structure of materials. For this reason, it is also known as Electron Spectroscopy for Chemical Analysis (ESCA). The working principle for XPS is the photoelectric effect. When X-ray photons are irradiated onto the material's surface, photoelectrons from the inner orbitals of the element are emitted. The detectors measure the kinetic energy of these emitted photoelectrons, which is correlated to the binding energy of the parent element by the following relation:

$$E_B = h\nu - E_k - \phi$$

Where E_B is the binding energy, $h\nu$ is the energy of the incident photon, E_K is the kinetic energy of the emitted photoelectron, and ϕ is the work function of the spectrometer (**Figure 2.3b**). The binding energy is characteristic of the elements and their chemical states. This allows for the identification and quantification of elements in the material's surface layer (up to 1-10 nm depth). For producing X-rays of fixed energy, an anode of aluminum (Al kα) or magnesium (Mg kα) is utilized. Due to the ultra-sensitive nature of this analysis, the whole experimental setup is maintained at ultra-high vacuum (typically around 10^{-9} to 10^{-10} torr) to maintain contamination-free pathways for emitted electrons. An electron energy analyzer is used to measure the kinetic energy of photoelectrons and their distribution. Finally, the XPS spectrum is generated by data captured by the detector. This instrument is combined with software to acquire and analyze data. The software also helps with peak fitting, quantification, and interpretation of the XPS spectra.

XPS is highly regarded for its ability to provide quantitative and qualitative information about the material's elemental composition and chemical states. It is extensively used in material science to analyze thin films, coating, and surface treatments. It is also used to investigate catalysts, adsorbates, and chemical reactions on surfaces. In electronics, it is used to study semiconductors, insulators, and conductive materials. This technique can detect all elements except hydrogen and helium because they don't contain inner shells of electrons.

2.1.6 Scanning Electron Microscope

A scanning electron microscope (SEM) is a powerful instrument that can provide detailed morphological images and elemental information of materials at high magnifications. This ability makes this instrument indispensable in material science, biology, and

nanotechnology. Where an optical microscope uses visible light for magnification, SEM operates by scanning the sample with a focused electron beam and detecting the generated signals from the interaction of electrons and sample atoms (**Figure 2.4**). The significantly smaller wavelength of electrons (~10^5 times smaller than visible light) offers SEM a greater resolution of up to 0.1 nm (compared to 200 nm for an optical microscope). The electron beam is emitted from the electron gun (usually tungsten filament or field emission gun) and, with the help of several well-positioned electromagnetic lenses, accelerated and focused into a fine probe. This probe interacts with the atoms present at the sample's surface, generating several signals, including secondary electrons, backscatter electrons, and auger electrons. These signals are collected by various detectors and provide important compositional information. Secondary electrons, emitted from near-surface regions, are used to generate high-resolution images of surface morphology. Backscattered electrons, reflected from deeper within the sample, can provide compositional contrast based on atomic number differences. The whole system is extremely sensitive and thus operated in a high-vacuum enclosure.

SEM is essential for examining the microstructure and composition of a wide range of materials. It provides high-resolution images that reveal fine surface details, making it crucial for studying the morphology of metals, polymers, ceramics, and biological specimens. In materials science, SEM aids in understanding failure mechanisms, analyzing fracture surfaces, and characterizing nanoparticles. SEM allows for the detailed visualization of cell structures, tissues, and microorganisms in biology.

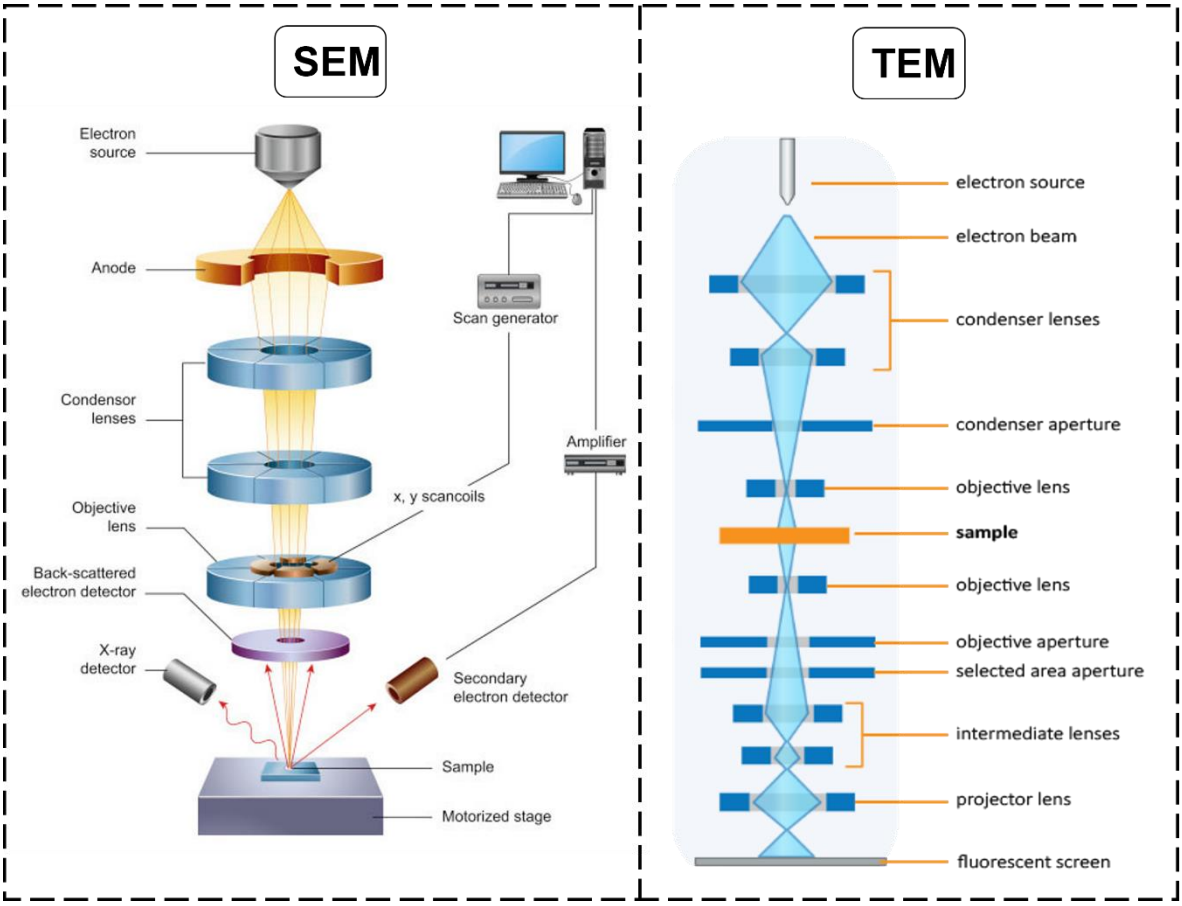

Figure 2.4 Schematic diagram of scanning electron microscope and transmission electron microscope. (Credit: https://www.nanoscience.com/techniques/scanning-electron-microscopy/)

2.1.7 Transmission Electron Microscope

Transmission Electron Microscope (TEM) allows for the visualization and characterization of the internal structure of materials at atomic or near-atomic resolution **(Figure 2.4**). TEM is widely used in various scientific fields, including materials science, biology, and nanotechnology, to provide detailed images and information about the fine structure and composition of specimens. TEM operates on the principle of electron transmission through a thin sample. An electron beam is generated by an electron gun and focused into a coherent beam using electromagnetic lenses. This focused beam passes through an ultra-thin specimen, where electrons interact with the sample atoms. The interactions produce various effects, including scattering and diffraction, which are then captured by a detector

(CCD or scintillator) to form an image or diffraction pattern. The resulting image provides information about the sample's structure, morphology, and composition. TEM requires that the sample prepared be less than 100 nm thick. It operates under a high vacuum to prevent electron scattering by air molecules.

TEM is highly valued for its ability to provide detailed structural and compositional information at the atomic scale. It is essential for characterizing the morphology and composition of nanoparticles, thin films, and complex materials. The technique's high resolution and versatility in studying a wide range of materials make TEM an indispensable tool in scientific research and technological development. Its ability to provide imaging and diffraction data enables comprehensive analysis, driving advancements in material science, biology, and nanotechnology.

2.1.8 Voltammetric Techniques

Voltammetric techniques are used to study the redox properties of chemical substances by measuring the current response as a function of an applied potential. These techniques provide valuable insights into the kinetics and mechanisms of electrochemical reactions, the identification and quantification of analytes, and the study of electron transfer processes. A typical voltammetric setup comprises an electrochemical cell with three electrodes **(Figure 2.5a**). The working electrode is the site where an electrochemical reaction takes place. The counter electrode (usually platinum) completes the circuit, and the reference electrode is used to measure the potential at the working electrode accurately. For this reason, the applied potential in voltammetry is referred to as “vs.” a specific reference. Voltammetry encompasses a range of methods, each tailored to particular types of analysis and offering unique advantages in different applications. This work uses Cyclic

Voltammetry (CV) and Differential Pulse Voltammetry (DPV) to probe the electrochemical processed at working electrode surface.

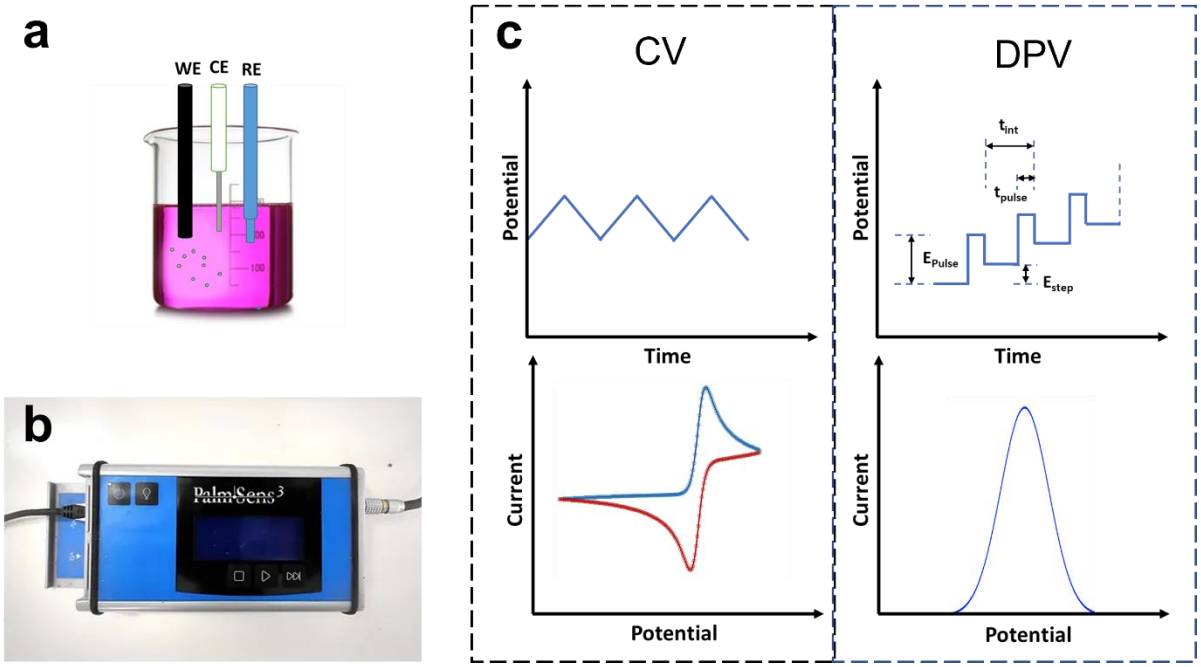

Figure 2.5 A conventional three-electrode electrochemical cell comprised of working electrode (WE), counter electrode (CE), and reference electrode (RE) (a), PalmSens 3 voltammetric analyzer (b), Voltage profile, and typical voltammograms for CV and DPV technique **(c)**.

2.1.1.1 Cyclic Voltammetry

Cyclic voltammetry is one of the most versatile electrochemical techniques for examining the redox behavior of chemical species. In this technique, the potential applied is swept linearly from an initial potential to an end potential and then reversed back to the initial potential at a fixed scan rate. The corresponding current response is recorded in a cyclic voltammogram (**Figure 2.5c**). This voltammogram presents several key features that can be interpreted to get an insight into the electrochemical behavior of electrodes. For instance, the difference between the potentials at which anodic and cathodic peak current is observed provides information about the reversibility of the redox process. The peak current is linearly related to the concentration of the electroactive species, described by the

Randels-Sevcik equation. The shape of the voltammogram also provides qualitative information about the system; a voltammogram symmetrical about the center describes a reversible process, whereas an asymmetrical or distorted voltammogram suggests the involvement of complex processes such as adsorption and coupled chemical reactions.

2.1.1.2 Differential Pulse Voltammetry

Differential Pulse Voltammetry (DPV) is an advanced electrochemical technique used for the sensitive and selective analysis of electroactive species. Unlike CV, where a linearly increasing potential is applied, DPV operates by applying a series of voltage pulses superimposed on a linear base potential to the working electrode (**Figure 2.5c**). The potential increases linearly at a fixed step rate. The current response is recorded twice during each pulse, just before and at the end of the pulse. The difference between these two measurements, or differential current, is plotted against the potential to generate a differential pulse voltammogram. The resulting voltammogram depicts peaks corresponding to the oxidation or reduction processes of the analyte. Compared to CV, DPV is highly sensitive, making it suitable for determining and estimating trace-level analytes with considerable accuracy. Due to the probe's differential nature, DPV produces sharper and better-resolved peaks than other voltammetric techniques.

2.1.9 Electrochemical Impedance Spectroscopy

Electrochemical Impedance Spectroscopy (EIS) measures the impedance of a system over a range of frequencies, providing insights into processes such as charge transfer, diffusion, and capacitive behavior. A small, alternating current voltage is applied to an electrochemical cell comprising three electrodes: the working electrode, the counter electrode, and the reference electrode. The resulting current response is measured at

varying frequencies. The impedance (Z) of the system is calculated as the ratio of the applied voltage (V) to the measured current (V) as a function of frequency (f):

$$Z\ (f) = \frac{V(f)}{I(f)}; \qquad Z(f) = Z' + iZ''$$

Impedance is comprised of both real resistance (Z') and imaginary resistance (Z") and is usually represented in a Nyquist plot or a Bode plot. Nyquist plot shows the imaginary vs real part of the impedance for different frequencies. It often results in semicircular patterns where each semicircle corresponds to a particular electrochemical process. Bode plot shows the magnitude of impedance (|Z|) and phase angle (θ) as a function of frequency, providing insight into the frequency-dependent behavior of the system. To interpret the impedance data, equivalent electrical circuits comprise resistors, capacitors, inductors, and other elements. We can model the different electrochemical processes through these equivalent circuits, such as charge transfer resistance, double-layer capacitance, and diffusion.

EIS technique is exclusively utilized to study the corrosion behavior of materials. It is used in battery research to analyze the internal resistance, charge-transfer resistance, and electrolyte behavior. It is also used to characterize electrodes, polymers, composites, and nanomaterials, providing insights into their electrical properties and charge storage capabilities. This technique's non-destructive nature and high sensitivity and versatility make it suitable for studying sensitive materials such as biological tissues and cells.

2.1.10 Glove Box

Battery research and manufacturing involves the use of extremely sensitive materials and chemicals. A glove box is a crucial piece of instrument that provides a controlled environment necessary for handling and assembling these components (**Figure 2.6a**). It

consists of a main chamber where all the assembly and handling are performed. This chamber is maintained at a high vacuum and is made of chemical-resistant and robust material. The front panel of this chamber is fitted with gloves so that materials inside can be moved without compromising the controlled environment. The glove box also contains a transfer chamber, which is used to remove or insert materials inside the main chamber without disrupting the internal atmosphere. The main chamber has several gas purification systems that continuously circulate and purify the internal atmosphere. Moisture and oxygen are removed by scrubbers, while filters trap particulates. The whole chamber is maintained at a slightly positive pressure to prevent contaminant ingress.

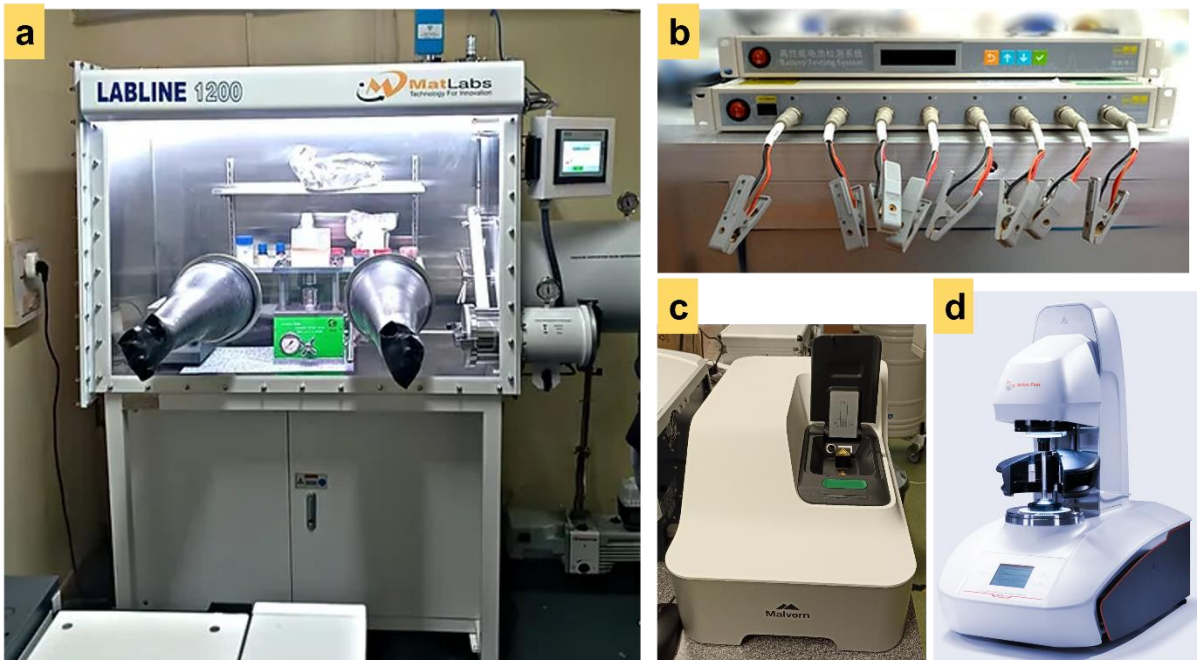

Figure 2.6 Photographs of Glove box (*MatLabs Labline1200*) **(a)**, battery tester (*Neware*) **(b)**, zetasizer pro (*Malvern Panalytics*) **(c)**, and rheometer (*Anton Paar*) **(d)**.

2.1.11 Battery tester

A battery tester is a crucial piece of equipment in both scientific and industrial battery innovation and manufacturing (**Figure 2.6b**). It performs a range of diagnostic tests to evaluate the performance, capacity, and overall health of batteries. These tests involve

open-circuit voltage, load test, capacity test, internal resistance measurement, and cycle test. In the Open-circuit voltage (OCV) test, the battery tester measures the voltage of the battery without any load. This test provides an indication of the battery's initial state of charge. In the Load test, a controlled load is applied to the battery, and the voltage drop is measured. This test evaluates the battery's current delivery capabilities. In the capacity test, the battery is discharged at a constant current until a predetermined cutoff voltage is reached. The capacity is calculated by evaluating the time taken in this process. This test is crucial for understanding the battery's energy storage capability. In cycling tests, the battery is subjected to repeated charging and discharging cycles to evaluate its long-term performance and durability. For this test, various parameters involving charging and discharging are defined, such as current and cutoff voltage. Following this, the battery tester records the battery voltage at regular intervals during the charging/discharging process. We can gain insights into the battery's behavior, performance, and charging mechanism by analyzing the voltage profile. This test also helps in understanding the degradation mechanisms in batteries. In real life, a battery needs to perform not only in ambient conditions but also in harsh environments that involve high temperatures. The battery tester is equipped with a setup to assess the performance of the battery under different thermal conditions.

2.1.12 Zetasizer

Zetasizer combines techniques such as Dynamic Light Scattering (DLS), Electrophoretic Light Scattering (ELS), and Static Light Scattering (SLS) to provide comprehensive data on colloidal systems, nanoparticles, and macromolecules (**Figure 2.6c**). In this work, we have made use of DLS. DLS measures particle size by analyzing the fluctuations in light scattering due to Brownian motion. When a laser beam passes through a particle

suspension, the particles scatter the light. The scattered light intensity fluctuates over time as the particles move, and these fluctuations are analyzed to determine the diffusion coefficient of the particles, which is then used to calculate their hydrodynamic diameter using the Stokes-Einstein equation. Its ability to provide detailed information on particle characteristics makes it an important analytical tool in pharmaceuticals, material science, chemistry, and nanotechnology.

2.1.13 Rheometer

A Rheometer measures the rheological properties of materials, including their viscosity, elasticity, and viscoelastic behavior (**Figure 2.6d**). The rheometer analyzes how materials respond to applied forces and provides essential insights into their flow and deformation characteristics under various conditions. Rheology involves subjecting a sample to controlled stress or strain and measuring its response. Depending on the type of material and the desired information, different rheometric tests can be conducted, including steady shear, oscillatory shear, and creep tests. For instance, in a steady shear test, the sample is subjected to a constant shear rate, and the resulting shear stress is measured to calculate the material's viscosity. Different geometries, such as parallel plates, cone-and-plate, or concentric cylinders, can be used depending on the sample type and the desired measurement.

The rheometer provides crucial information on the material's properties. It is essential for polymers, composites, gels, and cosmetics, making it a vital tool for quality control, product development, and fundamental research.

2.1.14 Texture Analyzer

A texture analyzer operates by applying controlled forces to a sample and measuring its response to deformation. The primary working principle involves the application of a force via a probe or fixture, which interacts with the sample under specific conditions. The sample's response is recorded as a force versus time or force versus distance curve, providing insights into its textural properties. The instrument performs tests like compression, tension, penetration, extrusion, and bending. This device is widely employed in food, pharmaceuticals, cosmetics, and materials science to assess attributes like hardness, cohesiveness, elasticity, and adhesion.

2.2 Experiments relating to BCN Assisted Electro-functionalization of SPE for Tryptophan Sensing

2.2.1 Materials

Boric acid (H_3BO_3), melamine ($C_3H_6N_6$), potassium ferricyanide ($K_3[Fe(CN)_6]$), hBN (avg. size <150 nm), and dopamine were purchased from Sigma-Aldrich Chemical Co (USA). L-tryptophan (TRP), uric acid, hypoxanthine, and liquid ammonia (25 %) were procured from CDH chemicals. Screen-printed electrodes (SPE) were purchased from Zensor Ltd. Phosphate buffers of different pH were prepared using sodium dihydrogen phosphate, disodium hydrogen phosphate, and phosphoric acid, following the protocol reported by Christian and Purdy. Deionized water (DI) was used in the preparation of all the aqueous solutions. All the reagents were of analytical grades and used as such without any further treatment.

2.2.2 Synthesis of Boron Carbon Nitride (BCN)

15 g of boric acid (H_3BO_3) and 11.808 g of melamine ($C_3H_6N_6$) were added to a 60 mL solution of 25% liquid ammonia. The resulting solution was then transferred to a 100 mL Teflon cylinder, which was subsequently placed and sealed in the steel autoclave (**Figure 2.7**). The mixture was then subjected to thermal treatment in the oven at 200° C for 24 h at a ramp rate of 5° C /min. Upon completion of the thermal treatment, the autoclave was cooled to room temperature, and the solution was centrifuged at 15000 rpm for 15 minutes to isolate the solid precipitates. The precipitates were repeatedly washed with DI and ethanol through centrifugation and then dried at 80° C overnight. The obtained material was weighed and crushed using mortar and pestle and used for subsequent experiments.

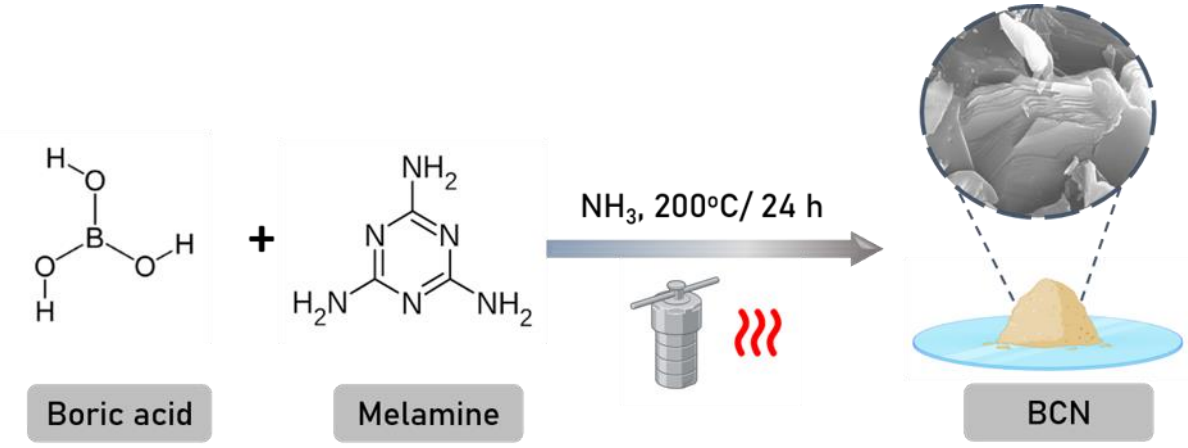

Figure 2.7 Schematic diagram showcasing the synthesis route for BCN nanomaterial.

2.2.3 Characterization techniques

The crystallographic information of synthesized BCN was obtained using the X-ray diffraction technique (Rigaku Miniflex 600, Japan) using a Cu-ka radiation source. The surface functionalities of BCN were investigated by performing Fourier-transform infrared (FTIR) spectroscopy in the wavenumber range of 500 – 4000 cm^{-1} with 4 cm^{-1} resolution using the Thermo Scientific^{TM} Nicolet iD7 spectrometer. The surface and morphological

information of BCN material, as well as the bare and modified ITO substrate, was extracted by employing a *ZEISS EVO* scanning electron microscope performed at 20kV, and the corresponding elemental analysis was performed by *51N1000 EDS system* (Oxford Instruments Nanoanalysis). K-Alpha, Thermo Fisher Scientific X-ray photon spectrophotometer equipped with a monochromatic Al-ka micro-focused X-ray source (100–4000 eV) was employed for elemental analysis of bare and modified SPEs. Electrochemical impedance spectroscopy (EIS) was performed in the frequency range of 0.1 - 10^6 Hz using MULTI AUTOLAB M204 (Metrohm Autolab). For validating the tryptophan concentration in the real samples, the absorbance spectra were recorded in the UV-visible range with the help of the Eppendorf bio-spectrometer. The electro-functionalization and the modified surface's thorough electrochemical characterization are performed using Palmsens3 voltammetric analyzer.

2.2.4 Electro-functionalization of Screen-Printed Electrode

Screen-printed electrodes were uniquely electro-functionalized with the BCN using cyclic voltammetry using a palmsens3 voltammetric analyzer. For carrying out the electro-functionalization, a stable suspension composed of 10 mg of the synthesized BCN material was dispersed in 20 mL of DI with the help of Labman PRO650 probe sonicator for one hour. The sonication was performed with 5s on and 10s off pulse setting. The resulting suspension was kept stationary for one day, and then the white-colored translucent supernatant was collected for further use. 0.5 mL of the prepared BCN suspension was added to a solution of 0.5 mL DI and 1.0 mL phosphate buffer (pH 7). 50 µL of this prepared solution was dropped over the SPE active surface. The cyclic voltammetry was then performed in the potential range of -1.0 – 1.5 V at a 100 mV/s scan rate. The number of scans required for the electro-functionalization of SPE was optimized to decide on the

modification protocol. The SPE was then rinsed with DI water and stabilized in the same potential range till three consecutive differential pulse voltammograms coincided perfectly.

2.2.5 Sample preparation and analytical techniques

Potassium ferricyanide redox couple was used to quantitatively assess the changes in the electrochemical performance of the screen-printed electrode (SPE) with and without BCN electro-functionalization. For this purpose, a stock solution of 1 mM potassium ferricyanide ($K_3Fe(CN)_6$) was prepared in deionized (DI) water. Tryptophan (TRP) stock solution of 1mM concentration was prepared by dissolving the required amount of TRP powder in DI water. The TRP solution was stored in a dark condition to prevent any light-induced oxidative degradation. For the quantitative analysis, a 2 mL solution for each TRP concentration was prepared using the dilution method. Briefly, the required volume of TRP stock solution was added to 1 mL phosphate buffer (pH 7). The total volume was then made to 2 mL by adding DI water. To investigate the potential interference of uric acid, ascorbic acid, and hypoxanthine with the electrochemical sensing of tryptophan, a test matrix was prepared. The concentration of tryptophan was fixed at 100 µM in all the solutions, while the concentration of interferents was varied between 25 to 200 µM. The electrochemical response was recorded using cyclic voltammetry (CV) and differential pulse voltammetry (DPV) by putting 50 µL of the desired TRP aliquot over the SPE. The CV was performed in the potential range of 0 - 1.0 V at a scan rate of 100 mV/s. DPV measurements were carried out in the potential range of 0.2 - 1.0 V at 20 mV/s. The SPE was rinsed with DI water and stabilized with PB7 in between subsequent.

2.2.6 Real sample assay and validation

To ensure the applicability of the prepared sensing platform for pragmatic purposes, TRP analysis was attempted in complex matrix like human urine, and egg white as the food sample. Tryptophan found in human urine originates from protein breakdown and metabolism. But, along with tryptophan, urine also contains a multitude of other biomolecules, which may affect its accurate determination. Therefore, the detection of tryptophan in urine is an excellent model for assessing the selectivity of the sensing platform. In the food sample, egg is recognized as a rich source of tryptophan, reportedly containing 143.1 mg of tryptophan per 100 g[136]. The presence of numerous other biomolecules makes the egg a suitable sample for testing the sensitivity and selectivity of our sensor.

2.1.1.3 Egg sample preparation

Chicken eggs were procured from the local market of Varanasi, India. For the purpose of tryptophan measurement, the egg white was separated from the yolk and taken into the beaker. 10 mL of phosphate buffer was added to 2 mL of egg white in the beaker and stirred with a magnetic stirrer for 30 minutes to form a colloidal solution. A differential pulse voltammogram was recorded by taking 50 µL of the prepared solution in the potential range of 0 – 1.0 V.

2.1.1.4 Urine sample preparation

The urine sample was collected from the healthy volunteer. The sample was diluted in the 1:9 ratios with the supporting electrolyte (phosphate buffer, pH 7). 50 µL of the diluted solution was pipetted out onto the modified SPE for recording the differential pulse voltammograms in the potential range of 0 - 1.0 V. For evaluating the accuracy of the

sensor; solutions were formulated, containing the same amount of urine sample, spiked with TRP of 20 and 100 µM concentration, respectively.

2.1.1.5 Data Validation

For validating the tryptophan concentration in the real samples, UV-visible spectroscopy was employed. For this purpose, five samples of known concentrations of TRP were prepared, and their absorbance was recorded at 280 nm to plot a calibration curve using a linear regression equation. The absorbance value of the egg white and urine samples at the same wavelength was recorded. The amount of TRP was then estimated by putting the observed absorbance value in the linear regression equation. The results from UV and the developed sensor were compared to check the error percentage and the validity of the sensor.

2.3 Experiments relating to Hexagonal Boron Nitride as Anode for Sodium-ion Battery

2.3.1 Materials

Boron nitride bulk (BNB) and boron nitride nanoplatelets (BNNP) were purchased from Sigma Aldrich and used as such. The topographical morphology of the materials was observed using a scanning electron microscope, and X-ray diffraction was employed to investigate their crystallinity. For this study, Bruker XRD diffractometer, model D8 Advance, was employed. SEM imaging of the samples was acquired with the help of JEOL Asia PTE Ltd JCM-6000 plus BenchTop Sem Neoscope.

2.3.2 Electrode preparation

To prepare the composite electrodes, a homogenous slurry was prepared by mixing 80 % of active material (BNB and BNNP, separately), 10 % of Super P carbon black and 10 % of poly (vinylidene fluoride) (PVDF) in N-methyl-2-pyrrolidone (NMP) using a Thinky mixer (ARV-310/ARV-310LED) at 2000 rpm, 30 kPa. The prepared slurry was then coated onto a clean, polished copper foil using a doctor's blade (thickness set at 120-micron) and dried overnight at 100°C. After calendaring, electrodes of 12 mm were punched, weighed, and vacuum dried overnight at 100^{o}C.

2.3.3 Electrochemical measurements

For the electrochemical investigations, 2032 type coin cells were fabricated inside the Argon-filled glovebox using BNB/BNNP electrodes (12 mm) as working electrodes and Na metal (14 mm) as pseudo-reference/counter electrodes. Two Celgard PP-3401 separators wetted with 20 µl electrolyte solution of $NaPF_6$ (1M) in propylene carbonate (PC), and 2% of fluoroethylene carbonate (FEC) were placed between the working electrode and the Na metal. The prepared cells were then taken out of the glovebox for electrochemical testing using galvanostatic discharge-charge cycling at 35 °C (Bio-logic Science equipment) in a potential window of 0.01-2.40 V. Three out of the total five prepared cells were used for each active material to ensure the repeatability of the storage capacity. The mass of active material, which was 4.440 mg and 0.624 mg for BNB and BNNP, respectively, was used to normalize all of the currents and capacities.

2.4 Experiments relating to Hexagonal Boron Nitride Decorated PP Separator

2.4.1 Materials

Boron nitride nanoplatelets (BNNP), sodium hexafluorophosphate (NaPF6), propylene carbonate (PC), and fluoroethylene carbonate (FEC) were purchased from Sigma Aldrich. The anhydrous solvents were dried over 4 Å molecular sieves inside the glovebox before use. The polypropylene 3401 separator was purchased from Celgard©. The topographical changes were observed using JEOL Asia PTE Ltd JCM-6000 plus BenchTop Sem Neoscope.

2.4.2 Separator preparation

To prepare the composite electrodes, a homogenous slurry was prepared by mixing 80% BNNP and 20% poly (vinylidene fluoride) (PVDF) in N-methyl-2-pyrrolidone (NMP) using a Thinky mixer (ARV-310/ARV-310LED) at 2000 rpm, 30 kPa. The prepared slurry was then coated onto a PP 3401 Separator (thickness set at 30-micron) and dried overnight at 60 °C. After mild calendaring, separators of 18 mm were punched, weighed, and vacuum-dried overnight.

2.4.3 Electrochemical measurements

For the electrochemical investigations, 2032-type symmetrical coin cells were fabricated inside the Argon-filled glovebox. To construct the symmetrical cells, Cu foils (12 mm) pre-deposited with two mAh cm^{-2} equivalent of Na metal were used both as cathode and anode. To deposit 2 mAh cm^{-2} equivalent of Na on the Cu foil, a cell with metallic Na as anode and Cu foil (12 mm) as cathode was constructed, and Na deposition was carried out

by applying a cut-off voltage of −1.0 V at a current density of − 0.5 mA cm−2 for 4h. Two Celgard PP-3401 separators wetted with 20 µl electrolyte solution of NaPF6 (1 M) in propylene carbonate (PC) and 2% of fluoroethylene carbonate (FEC) were placed between the two electrodes. The prepared cells were then taken out of the glovebox for electrochemical testing using galvanostatic discharge-charge cycling at 35 °C (Bio-logic Science equipment). The reversibility of Na was measured by depositing-stripping 80% of Na at ± 1 mA cm^{-2} in a potential window of −1.0 to 1.5 V.

2.5 Experiments relating to Conductive r(GO/BSA) Hydrogel for Rapid Chronic Diabetic Wound Healing

2.5.1 Materials

Bovine Serum Albumin (BSA), graphite, sulfuric acid (H_2SO_4, 98%), sodium nitrate ($NaNO_3$), potassium permanganate ($KMnO_4$), hydrochloric acid (HCl, 30%), Hydrogen peroxide (H_2O_2, 30%), and L-ascorbic acid were purchased from Sigma-Aldrich. Streptozotocin (STZ) and citrate buffer were purchased from Sigma-Aldrich. Dimethyl sulfoxide anhydrous (DMSO) and Fetal Bovine Serum (FBS) were procured from SRL. LB broth and nutrient agar media were purchased from HiMedia laboratories. The NIH-3T3 cell line was procured from NCCS Pune. Deionized (DI) water (> 18MΩ) was used to prepare all aqueous solutions. All the reagents were used as such without further purification.

2.5.2 Synthesis of Graphene oxide

Graphene oxide was prepared using a modified Hummer's method, using graphite as a precursor[34]. Briefly, in a three-neck flask, 1 g of graphite was mixed with 150 mL of H_2SO_4 (conc.) and 1.5 g of $NaNO_3$ for 15 min under constant magnetic stirring while maintaining

temperature under 5°C. Following this, 6g of $KMnO_4$ was very slowly added to the mixture over a period of 30 minutes under continuous stirring until the mixture turned into a dark green paste. The prepared mixture was diluted with 180 mL of DI water, accompanied by a dropwise addition of H_2O_2. The resulting dark brown mixture was filtered and washed with HCl and DI water until the neutral pH was achieved. The mixture was further sonicated and centrifuged to remove excess $KMnO_4$ and metal ions. The sediment was air-dried overnight to obtain graphite oxide. Finally, the obtained powder was dispersed in DI water and sonicated in a water bath to obtain graphene oxide dispersion.

2.5.3 Synthesis of r(GO/BSA) hydrogel

Lyophilized BSA powder was dissolved in DI water at 300 mg/ml concentration. A stock solution of 10 mg/ml Graphene oxide was prepared in DI water. Next, an assortment of samples of 200 mg/ml BSA was prepared in Petri dishes with varying concentrations of GO (namely 0.1, 0.5, and 1% (w/v)). The petri dishes were incubated in a hot air oven preheated at 80°C for 30 minutes. After incubation, the obtained GO/BSA hydrogels were placed in ambient conditions to bring them to room temperature. A control hydrogel was also prepared, where instead of GO, an equivalent amount of DI was added to maintain a constant concentration. Eventually, GO/BSA hydrogels were chemically reduced to r(GO/BSA) by incubation in a 2 $mgmL^{-1}$ ascorbic acid solution at 37 °C for 24 h. The hydrogels were washed several times with DI water and stored at 4°C for further application. For further discussion, the hydrogels were named BSA for control $(GO/BSA)_x$ and $r(GO/BSA)_x$ hydrogel, respectively, where x represents the concentration of GO in the sample hydrogel.

2.5.4 Graphene Oxide Characterization

The optical absorbance of the prepared graphene oxide (GO) was recorded using an *Eppendorf biospectrometer* in the wavelength range of 200-800 nm. To obtain detailed crystallographic information, X-ray diffraction technique analysis was performed using a *Rigaku Miniflex 600* with a Cu-kα radiation source. Raman spectroscopy was conducted to analyze the structural defects of GO. DLS measurements were performed using *Malvern Panalytical Zetasizer Pro* to examine the hydrodynamic size distribution and polydispersity index (PDI) of graphene oxide. The surface morphology of GO samples was examined using a scanning electron microscope (*NovananoSEM*), which provided detailed images of surface features. Furthermore, transmission electron microscopy (*Tecnai G2 20 TWIN*) was utilized to investigate the morphology at a higher resolution.

2.5.5 Hydrogel characterization

The porosity and cross-sectional surface morphology of the hydrogels were investigated using an *EVO MA15/18* scanning electron microscope. Pore distribution data were analyzed and tabulated using ImageJ software. The rheological properties of the prepared hydrogels were measured using a parallel plate geometry setup in an *Anton Paar MCR 72 Rheometer***.** Initially, the linear viscoelastic range (LVR) was determined by applying a constant frequency of 10 rad/s. Subsequently, a frequency sweep was performed across a range of 0.1 rad/s to 10 rad/s at a constant strain in LVR to determine the storage and loss modulus, G’ and G” respectively. Additionally, the shear thinning behavior was investigated in the shear rate range of 0.1 – 100 s^{-1}.

The mechanical strength of prepared hydrogels was studied through compression tests performed on a texture analyzer (*Shimadzu, Japan*) with a maximum load capacity of 500 N. For these tests, the hydrogels were cut in cylindrical shape with a diameter of 10mm

and a height of 5mm. The compression measurements were carried out at a constant speed of 1mm/min. Additionally, cyclic compression tests were performed by subjecting hydrogels to 50% deformation over three cycles.

The swelling ratio and water retention properties of prepared hydrogels were investigated. For this purpose, the lyophilized samples were first soaked in DI water for 24h to allow them to reach equilibrium swelling. Following this, the samples were carefully removed from the water, and superficial water was removed using kimwipes. The swollen samples were then weighed.

The swelling ratio, S, was calculated using the formula,

$$S = \frac{w_t - w_0}{w_0}$$

Where w_0 and w_t are the weights of dry and swollen hydrogel samples, respectively.

The water-retaining ratio (WRR) was also calculated for all hydrogels. For this, swollen hydrogels were periodically weighed over a time period of 15 days at an interval of 2 days. Each measurement was conducted in triplicate for all hydrogel samples.

Conductivity measurements were performed using a digital multimeter (*FLUKE 287 true rms multimeter*). For this purpose, the hydrogel samples were cut into cuboid shapes with fixed lengths and cross-section areas. Triplicate readings for resistance were measured at the end points of each sample and averaged. The conductivity, σ, was computed using the following relation:

$$\sigma = \frac{L}{R.a}$$

Where R is the measured resistance, L and a are the length and cross-sectional area of the sample.

To measure the ionic conductivity of the prepared hydrogels, electrochemical impedance spectra were recorded by applying an alternate sinusoidal potential of 10 mV in the frequency range of 1-10^5 Hz using a computer-assisted MULTI AUTOLAB M204 (*Metrohm Autolab*) system. For this purpose, disc-shaped samples of 10mm diameter and 5mm thickness were prepared and placed between two parallel silver electrodes.

2.5.6 Antibacterial activity assay

The antibacterial efficacy of the r(GO/BSA) composite hydrogel was evaluated against Gram-positive (S. aureus) and Gram-negative (E. coli) bacteria using the agar disc diffusion method and kinetic growth inhibition studies. Overnight cultures of E. coli and S. aureus were grown in Luria-Bertani (LB) medium and incubated at 37°C. These cultures were then diluted to an optical density (OD) of 0.6 (at 600 nm) and treated with various concentrations of the rGO-BSA hydrogel. As a positive control, ampicillin was used. The treated cultures were incubated at 37°C, and the optical density was measured after 24 hours using a microplate reader.

For the agar disc diffusion assay, 200 µL of each bacterial culture (OD 0.6) was evenly spread onto the agar plates. Whatman filter paper discs (6 mm in diameter) were soaked in 1 mg/mL hydrogel solutions and placed on the plates. Additionally, the disc soaked in ampicillin solution served as a positive control. The plates were incubated at 37°C for 24 hours. The inhibition zones around the discs were measured to determine antibacterial efficacy.

2.5.7 In vitro study

The biocompatibility of BSA, GO/BSA, and r(GO-BSA) hydrogel formulations was examined using the NIH-3T3 cell line and assessed via the MTT assay. NIH-3T3 embryonic mouse fibroblast cells were seeded in 96-well plates at a density of $1x10^4$ cells per well in 100 µL of complete medium and incubated for 24 hours. Post incubation, the cells were treated with three concentrations (5µL/mL, 10µL/mL, and 20µL/mL) of each

formulation for 24, 48, and 72 hours to assess the time-dependent effects of the formulation on cell viability. Following treatment, the medium was replaced with 100µL of MTT solution (0.5 $mgmL^{-1}$), and the cells were incubated for an additional 4 hours at 37°C in a 5% CO_2 atmosphere to allow the yellow MTT tetrazolium salt to be reduced by viable cells to purple formazan crystals. Following this, the MTT solution was carefully removed, and 100µL of DMSO: MeOH (1:1) solution was added to dissolve the formazan crystals. The absorbance of the resulting-colored solution was measured at 570 nm using a multi-plate reader.

The cell viability was calculated by the following relation:

$$\%\ cell\ viability = \frac{A_S}{A_C} * 100$$

Where A_S and A_C represent the absorbance of the treated sample and control at 570 nm, respectively.

2.5.8 In vivo study

A rat model was used to conduct the in-vivo assessment of composite hydrogel. Rats were acclimatized under standard conditions with free access to commercial pellet food and water. Diabetes was induced in rats using streptozotocin (STZ) injection at a 60 mg/kg body weight dose dissolved in a 0.1M citrate buffer (pH 4.5). To confirm the successful induction of diabetes, blood glucose levels were monitored three days post-STZ injection. Blood samples were obtained via tail vein sampling. Only those rats with fasting blood glucose levels above 250 mg/dL were considered diabetic and included in the study. On the 8th day post-STZ injection, a full-thickness excisional wound was created on the rats' backs and disinfected with 70% ethanol. Diabetic animals were divided into four groups: (1) positive control (antibiotic ampicillin was applied), (2) negative control (no treatment),

(3) BSA hydrogel-treated wounds, and (4) r(GO/BSA) composite hydrogel-treated rats. Treatments were applied topically every other day until the complete wound healing was observed. Throughout the experimental period, blood glucose levels and body weight were measured regularly to monitor the health status of rats. At the experiment's conclusion, rats were fasted overnight to stabilize the metabolic rate. Subsequently, the animals were sacrificed as per the guidelines of the ethics committee, and wound tissues were excised for histopathological analysis.